A Novel Fluorescent Probe That Senses the Physical State of Lipid Bilayers

Hirotaka Sasaki and Stephen H. White*
Department of Physiology and Biophysics, University of California at Irvine, Irvine, California

ABSTRACT Cell membrane lipids and proteins are heterogeneously distributed in the membrane plane. In recent years, much attention has been paid to the heterogeneous distribution of the lipid components, particularly the formation of cholesterol-rich domains that are thought to be important in signaling processes. This has led to renewed interest in the phase diagrams of complex lipid mixtures, such as three-component mixtures containing phospholipids and cholesterol. We report here a novel fluorescent probe (NBD-R595) that is useful for exploring the phase behaviors of one-, two-, and three-component large unilamellar vesicles. In one-component fluid-phase membranes, the probe has the expected spectral characteristic of monomeric 7-nitrobenzo-2-oxa-1,3-diazol, with a fluorescence maximum of 540 nm when excited at 470 nm. But below the gel-to-liquid crystalline phase transition temperature, an additional emission peak appears at ~610 nm, because of Förster resonance energy transfer from NBD-R595 monomers to NBD-R595 Jelley aggregates of limited size formed by the association of 7-nitrobenzo-2-oxa-1,3-diazol moieties. This may be the first report of Förster resonance energy transfer from a single fluorophore in two different physical states. In a test of the probe, we found NBD-R595 to be remarkably sensitive to the molar composition of large unilamellar vesicles formed from cholesterol, distearoylphosphatidylcholine, and dioleoylphosphatidylcholine.

INTRODUCTION

Lipids and proteins coexist in biomembranes. The widely cited fluid-mosaic membrane concept (1) describes biomembranes as a mixture of integral membrane proteins distributed randomly in a fluid lipid bilayer. However, a growing number of physical and biological experiments suggest that the proteins and lipids can form segregated structural domains in the bilayer, because of the large area occupancy of proteins (2) and specific lipid-lipid, lipid-protein, protein-protein, and protein-cytoskeleton interactions (3–5). Much attention has been paid in recent years to the heterogeneous distribution of the lipid components, particularly the formation of cholesterol-rich domains that are thought to be important in signaling processes (6). This has renewed interest in the phase diagrams of complex lipid mixtures, such as three-component mixtures of cholesterol with two phospholipid species. The development of phase diagrams for such mixtures is notoriously demanding. The phase behavior of several three-component cholesterol/phospholipid mixtures have been reported based mainly on fluorescence microscopic studies using giant unilamellar vesicles (GUVs) (7–14) (see review by Feigenson (3)). Unlike GUVs, large unilamellar vesicles (LUVs) are too small for fluorescence microscopy imaging and generally require the use of calorimetric and diffraction methods for phase behavior analysis (15). We report here a novel lipopolysaccharide-based fluorescent probe that is useful for exploring the phase behavior of one-, two-, and three-component LUVs, in conjunction with other physical methods.

Lipopolysaccharides (LPSs) are amphiphilic glucosamine-based phospholipids found in the outer bilayer leaflet of the outer membranes of most gram-negative bacteria (16). LPSs activate the immune system in mammals and are considered to play a key role in human septic shock syndrome (16,17), one of the major causes of death in U.S. intensive-care units (18). Recent studies on the mechanism of LPS-induced immunostimulation have focused attention on the roles of monomeric and multimeric forms of LPS in immune activation (19–21). In the course of characterizing the aggregation behavior of an exceptionally pure monomolecular LPS species known as Kdo_2-Lipid A (22), we became interested in the partitioning of LPS into phospholipid bilayers, which is most easily studied by use of fluorescence methods. (23).

We prepared a fluorescent LPS by covalently linking 7-nitrobenzo-2-oxa-1,3-diazol (NBD) to each of the two amine groups of LPS from *Salmonella minnesota* R595 (Fig. 1). This new probe, which we term NBD-R595, readily partitioned into fluid-phase LUVs accompanied by the expected blue-shifted NBD fluorescence maximum (λ_{max}) when excited at 470 nm. We soon discovered that, below the gel-to-liquid crystalline phase transition of LUVs, a second fluorescence peak with $\lambda_{max} \approx 610$ nm appeared. Further studies, reported here, suggested that this 610 nm emission peak results from Jelley aggregates (J-aggregates) of limited size and coherence length formed by associations of the NBD moieties of NBD-R595.

Archetypal J-aggregates (24,25) are formed through intermolecular dipolar coupling among excited-state fluorophores (26) organized into ordered multimolecular arrays. For example, J-aggregates of pseudoisocyanine dye form arrays of 20 to 10^6 monomers (27–29), but with optical coherence domains of typically <20 molecules (30,31). J-aggregates

Submitted October 6, 2008, and accepted for publication March 18, 2009.

*Correspondence: stephen.white@uci.edu

Editor: Enrico Gratton.

0006-3495/09/06/4631/11 $2.00

doi: 10.1016/j.bpj.2009.03.003

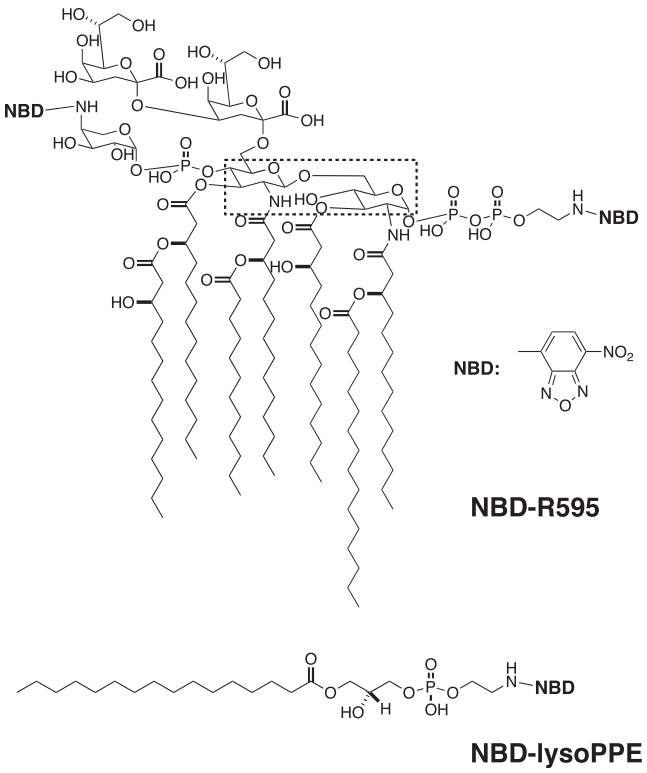

FIGURE 1 Chemical structures of NBD-R595 and NBD-lysoPPE. Saccharides referred to as ''core sugars'' (39) are surrounded by a dashed square.

can be formed in aqueous solutions (24,25,30,32), at silver halides interfaces (33), micelles (31,34), or lipid membranes (29,34). Delocalization of excitons within coherent domains (26), exciton-vibration interactions (35,36), and exciton-phonon interactions (36,37) give rise to the spectroscopic hallmarks of J-aggregates: an intense and narrow red-shifted absorption band (J-band) relative to the monomer band (24,25) and an extremely small Stokes shift (several nm) (32,34,38). We show below that NBD-R595 adsorbed to lipid vesicles has modest, but clear, J-aggregate spectroscopic characteristics, which suggest aggregates with small coherence size. The existence of two absorption bands ($\approx$470 and $\approx$570 nm) leads to the novel situation of Förster resonance energy transfer (FRET) between monomeric NBD moieties and NBD J-aggregates that yields a fluorescence peak at ~610 nm. FRET between different J-aggregate species in membranes has been reported (29), but as far as we can establish, this is the first report of FRET between a single fluorophore in two different states on the surface of membranes.

The presumed small coherence size of the J-aggregate domains apparently make their fluorescence exquisitely sensitive to the local LUV lipid environment, which we demonstrate by a partial exploration of a published phase diagram for a three-component phospholipid/cholesterol system determined for GUVs (3). The results suggest that NBD-R595 will be generally useful as an aid for studying the phase behavior of lipid mixtures.

MATERIALS AND METHODS

Materials

LPS from a deep-rough mutant strain of *S. minnesota* R595 (R595) was purchased from Sigma Chemical Co. (St. Louis, MO). Dipalmitoylphosphatidylcholine (DPPC), distearoylphosphatidylcholine (DSPC), dioleoylphosphatidylcholine (DOPC), cholesterol, and 1-palmitoyl-lysophosphatidylethanolamine (lysoPPE) were purchased from Avanti Polar Lipids, Inc. (Alabaster, AL). 4-Chloro-7-nitrobenzo-2-oxa-1,3-diazole (NBD-Cl) was from Molecular Probes, Inc. (Eugene, OR). Triethylamine was obtained from Acros Organics (Geel, Belgium). Dulbecco's phosphate buffered saline (DPBS) without Ca^{2+} and Mg^{2+} was from HyClone (Logan, UT). All chemicals were used as purchased without further purification.

Rationale for derivatization of *S. minnesota* R595

LPSs expressed by bacteria are chemically heterogeneous but have common structural features: a hydrophilic polysaccharide attaches to a hydrophobic ''endotoxic principle'' termed Lipid A. The heterogeneity of LPSs is mainly generated by the variation in the number of repeating saccharide units, named O-antigen, and by substitutions in the fatty-acid chains in the Lipid A region (16,39). LPS of so-called rough mutant strains do not have the O-antigen, but, rather, they have only 2–15 nonrepeating ''core'' oligosaccharides (39), which are characterized by ''chemotypes'' with decreasing lengths of the ''core sugars'', known as Ra, Rb, Rc, Rd, and Re (40). R595, which is an Re LPS with two core sugars, has been reported to be chemically homogeneous from deoxycholate and sodium dodecyl sulfate gel electrophoresis studies (41–43), probably because of the lack of heterogeneous O-antigen. Taking advantage of this homogeneity and two primary amine groups in the molecule, R595 was chosen for derivatization with NBD.

Labeling and purification of NBD-R595 and NBD-lysoPPE

NBD-R595 and NBD-lysoPPE were synthesized by covalently attaching the NBD probe to the two primary amino groups of R595 and lysoPPE. A procedure reported by Stillwell et al. was used to do these syntheses (44). Two mg of R595 (or 6.4 mg of lysoPPE) was dissolved in 0.5 mL (1 mL for lysoPPE) of chloroform-methanol (1:1, v/v) containing 10 μL (or 20 μL for lysoPPE) triethylamine. After addition of 2 mg (13 mg for lysoPPE) of NBD-Cl, the mixture was vigorously shaken and stored in the dark for 21 h at room temperature. The reaction products were dried under nitrogen stream and then dissolved in chloroform.

The fluorescent lipids were purified by preparative silica gel thin-layer chromatography in a solvent system consisting of 80% $CHCl_3$ + 20% CH_3OH for NBD-R595, and 65% $CHCl_3$ + 30% CH_3OH + 2.5% H_2O + 2.5% triethylamine for NBD-lysoPPE. Unreacted R595 and lysoPPE remained near the origin (Rf ~0.1). A partially labeled compound of NBD-R595, in which only one of the primary amines was attached by NBD, was not detected on thin-layer chromatography plates. The doubly-labeled NBD-R595 and NBD-lysoPPE migrated with Rf ~0.3 and Rf ~0.6 in each solvent system, respectively. Purified NBD-R595 (0.8 mg) and NBD-lysoPPE (3.7 mg) were obtained as solids and dissolved in methanol to make stock solutions. The concentrations of the stock solutions were determined spectrophotometrically using an extinction coefficient of 25,000 $M^{-1}cm^{-1}$ for NBD at 480 nm (45). The concentration of NBD-lysoPPE was 1.5 mM. By comparing the spectrophotometrically determined NBD concentration (277 μM) to the estimated concentration of NBD-R595 from its weight (143 μM), double labeling of NBD-R595 was confirmed. The emission spectrum of NBD-R595 in aqueous buffer had a simple log-normal shape (see Fig. S1 in the Supporting Material), which is generally agreed to be emission spectra from single NBD fluorophores (46,47).

Sample preparation

For fluorescence and UV/Vis absorbance measurements, LUVs of diameter 0.1 μm were prepared by extrusion (48) of 20 mM of lipid suspensions in DPBS (pH 7.2) using DOPC, DPPC, DSPC, DSPC-DOPC, or DSPC-DOPC-cholesterol mixtures. The conditions for extrusions of DOPC, DPPC, DSPC, DSPC–DOPC and DSPC-DOPC-cholesterol suspensions were 25°C (250 psi), 50°C (250 psi), 60°C (600 psi), 60–80°C (600 psi) and 60–80°C (600 psi), respectively. Lipid concentrations of the extruded lipid were determined according to the procedure of Bartlett (49). Samples were prepared by adding the required amounts of NBD-R595 (143 μM) or NBD-lysoPPE (1.5 mM) stock solutions to DPBS in the presence or absence of lipid LUV*s*. The final concentrations of NBD-R595 and NBD-lysoPPE for fluorescence measurements were typically set to be 0.92 μM and 2.0 μM, respectively. NBD-R595 and NBD-lysoPPE concentrations for UV/Vis absorbance measurements ranged from ~2 to ~11 μM.

Fluorescence measurements

Fluorescence measurements were performed using an SLM-Aminco 8100 steady-state fluorescence spectrometer (Jobin Yvon, Edison, NJ) modified by Olis, Inc. (Bogart, GA). The instrument was equipped with double-grating excitation and single-grating emission monochromators. All measurements were made in 2 mm × 10 mm cuvettes. Cross-orientation of polarizers was used, with excitation polarization set to horizontal and emission polarization set to vertical, to minimize the scattering contribution from vesicles and to eliminate spectral polarization effects in monochromator transmittance (23). Excitation spectra were obtained by averaging 8–16 scans collected over a 370–600 nm or 390–620 nm range using 1-nm steps and a 1-s integration time per step. Emission spectra were collected by averaging 10–64 scans collected over a 480–700 nm, 550–720 nm, or 580–720 nm range, also using 1-nm steps and a 1-s integration time per step. Excitation slits were 4 nm and emission slits were 8 nm for all fluorescence measurements. Before collecting data, samples were stored at the required temperatures for at least 30 min, and equilibration was confirmed by lack of changes in spectral traces between 15 scans at each temperature. For detection of the phase transition temperatures of DPPC, to avoid the effect of the hysteresis based on the kinetic nature of phase transitions (50), temperatures were changed in upward-and-downward mixed sequences with increments and decrements of 0.5–2.0°C between 18.5 and 44°C.

UV/Vis absorbance measurements

UV/Vis absorbance measurements were performed with a Cary 3E spectrophotometer (Varian Analytical Instruments, Sugar Land, TX) at room temperature. Each spectrum was obtained as an average of 12 scans, recorded with 1-nm steps and a 0.2-s integration time per step.

RESULTS

We began our characterization of NBD-R595 by examining systematically its spectroscopic properties in aqueous buffer in the presence and absence of LUVs. Because NBD-R595 is amphipathic (Fig. 1), we first estimated its critical micelle concentration (CMC) (see Fig. S2). We then determined water-to-bilayer partition coefficients to establish that the probe was predominantly in the lipid bilayer phase, and that the probe existed as monomers in the aqueous phase. The fluorescence of NBD-R595 partitioned into lipid vesicles was then examined above and below gel-to-liquid-crystalline phase transition, which revealed the appearance of an additional fluorescent peak at $\approx$610 nm in the gel phase. For single-component vesicles, this second peak was used to estimate pretransition and main-transition temperatures. In an exploration of the origin of the red-shifted peak, we surmised that it likely originates from membrane-bound J-aggregates with small coherence domains. Finally, we explored the J-aggregate fluorescence in various DSPC/DOPC/cholesterol mixtures to evaluate the sensitivity of the probe to the physical state of three-component LUVs.

Characteristics of NBD-R595 in aqueous buffer

The emission spectrum of NBD-R595 in aqueous buffer had a λ_{max} of 565 nm when excited at 470 nm (see Figs. S1 and S2). As expected, the amphiphilicity of NBD-R595 in water promoted aggregation above a CMC value. The CMC of NBD-R595 at 37°C, estimated from temperature-dependent changes in emission spectra, was found to be >92 nM but <198 nM (see Fig. S2). Importantly, Fig. S2 shows the absence of the 610 nm emission peak in both monomers and aggregates. NBD-R595 partitioned strongly into LUVs, regardless of lipid species or lipid phase state. For example, the partition coefficients, determined by fluorescence titration (51), for fluid DOPC, fluid DPPC, and nonfluid DPPC LUVs, were estimated to be 1×10^6, 1.2×10^6, and 1.5×10^6, respectively (data not shown). It was thus possible to assure for all of our measurements that NBD-R595 was present overwhelmingly in the membrane-bound form, and that the low concentrations in the aqueous phase were below the CMC.

Spectral characteristics of NBD-R595 in the presence of one-component lipid LUVs

Fig. 2 *a* shows typical emission spectra of NBD-R595 in the absence and presence of DOPC vesicles, which are fluid at all temperatures above 0°C. Also shown are emission spectra of NBD-lysoPPE in the presence and absence of DOPC vesicles. Both the NBD-R595 and the NBD-lysoPPE curves have simple log-normal shapes, show intensity increases in the presence of DOPC vesicles, and show blue shifts in λ_{max}. The blue-shift is larger for NBD-lysoPPE in the presence and absence of vesicles, probably because of deeper NBD penetration into bilayers and micelle formation in the absence of vesicles. These spectral changes, which are typical for NBD compounds (46,47), indicate that both NBD-R595 and NBD-lysoPPE partition into the nonpolar environment of the vesicles (47).

Unlike the emission spectrum for DOPC vesicles, the emission spectrum for NBD-R595 partitioned into DPPC LUV membranes varied dramatically and reversibly with temperature. DPPC forms a fluid L_α phase above the gel-to-liquid crystalline phase transition temperature ($T_m \approx 41$°C) and a nonfluid gel phase below the T_m. Above the DPPC T_m, the NBD-R595 emission spectrum had a simple log-normal shape with $\lambda_{max} = 540$ nm when excited at 470 nm. Below the T_m, an additional peak appeared at 610 nm (Fig. 2 *b*). This new peak was not observed at any temperature (5°–60°C) for any concentration of NBD-R595 in aqueous

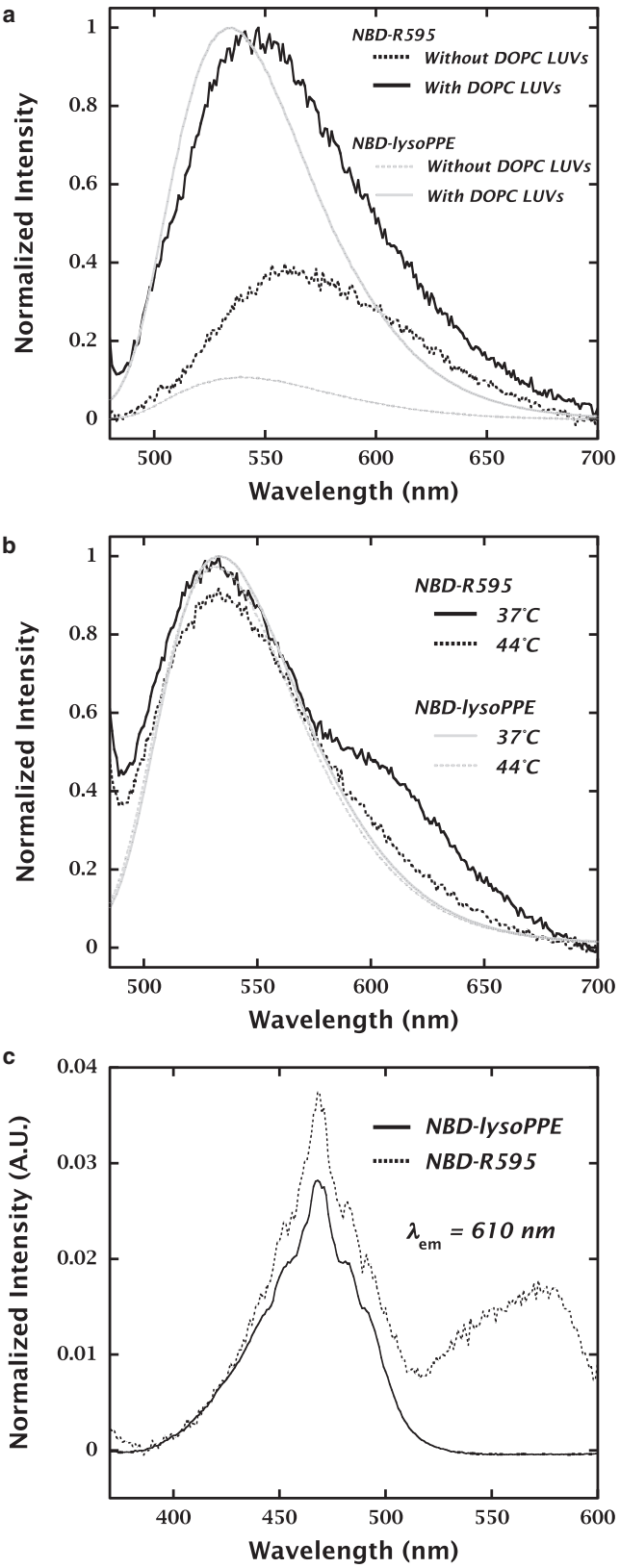

FIGURE 2 (*a*) Emission spectra of NBD-R595 (0.92 μM) and NBD-lysoPPE (2.0 μM) in DPBS (pH 7.2) in the absence (*dotted line*) and presence (*solid line*) of DOPC LUVs (99 μM) at 37°C. Sets of black and gray lines represent the spectra collected for NBD-R595 and NBD-lysoPPE, respectively. DOPC is in L_α phase at 37°C. Excitation wavelength was set to 470 nm. Fluorescence data from each probe were normalized using the maximum intensity of the spectrum in the presence of DOPC LUVs. (*b*) Emission spectra of NBD-R595 (0.92 μM) and NBD-lysoPPE (2.0 μM) in DPBS (pH 7.2) in the presence of DPPC LUVs (326 μM) below and above the T_m of DPPC (~41°C). Solid-black and dotted-black lines represent the NBD-R595 spectra at 37°C ($<T_m$) and at 44°C ($>T_m$), respectively. Solid-gray and dotted-gray lines represent the NBD-lysoPPE spectra at 37°C and 44°C, respectively. Excitation wavelength was 470 nm. Fluorescence data from each probe was normalized using the maximum intensity of the spectrum at 37°C. The decrease in spectral area at the higher temperature was because of the temperature dependence of NBD's quantum yield (63). (*c*) Comparison of the excitation spectra of NBD-R595 (0.92 μM) and NBD-lysoPPE (10 μM) in DPBS (pH 7.2) with DPPC LUVs (703 μM) at 37°C. The spectra of NBD-R595 and NBD-lysoPPE are drawn as dotted and solid lines, respectively. Fluorescence intensities were normalized to account for differences in concentration of the NBD-labeled lipids. Emission wavelength was 610 nm. In contrast to results with NBD-R595, NBD-lysoPPE had no excitation peak around 570 nm, even in the presence of DPPC vesicles.

buffer in the absence of lipid vesicles, suggesting that NBD-R595 is sensitive to the phase state of the lipid. Importantly, the NBD-lysoPPE fluorescence showed no significant changes with the phase state of the lipid (Fig. 2 *b*). The excitation spectrum of NBD-R595 partitioned into DPPC LUV below T_m revealed a second peak not observed in the spectrum of NBD-lysoPPE (Fig. 2 *c*).

Determination of phase-transition temperatures of one-component membranes using NBD-R595

Several spectral parameters for the 610 nm red-shifted emission peak varied drastically with temperature (see Fig. S3). Variations in spectral parameters as a function of temperature were analyzed by decomposing (23,52) the emission spectra of NBD-R595 into log-normal curves (see Fig. S4). Among the parameters, we found that the ratio of the intensity at 610 nm to that at 540 nm (I_{610}/I_{540}) and at the peak position of the red-shifted peak (λ_{max2}) provided good estimates for T_m (Fig. 3 *a*) and the pretransition temperature T_{pre} (Fig. 3 *b*), respectively. The pretransition is a minor structural transition from L'_β phase to rippled gel (P'_β) phase, which includes a change in tilt angles of hydrocarbon chains with respect to the bilayer normal (53). T_{pre} and T_m determined from sigmoidal fits were 34.1 $\pm$ 0.1 and 40.5 $\pm$ 0.1°C, respectively, which are somewhat different from values determined calorimetrically. Furthermore, the transitions are broader than observed calorimetrically.

Origin of the red-shifted emission peak

The excitation and emission spectra of NBD-R595 and NBD-lysoPPE (Fig. 2) suggested the possibility of FRET between NBD moieties of NBD-R595 in two different physical states. Given the similarities of the emission spectra of NBD-R595 in the presence of DPPC LUVs above T_m (Fig. 2 *b*) and NBD-lysoPPE under all conditions (Fig. 2, *a* and *b*), one of the states seems likely to be monomeric NBD-R595. But we first

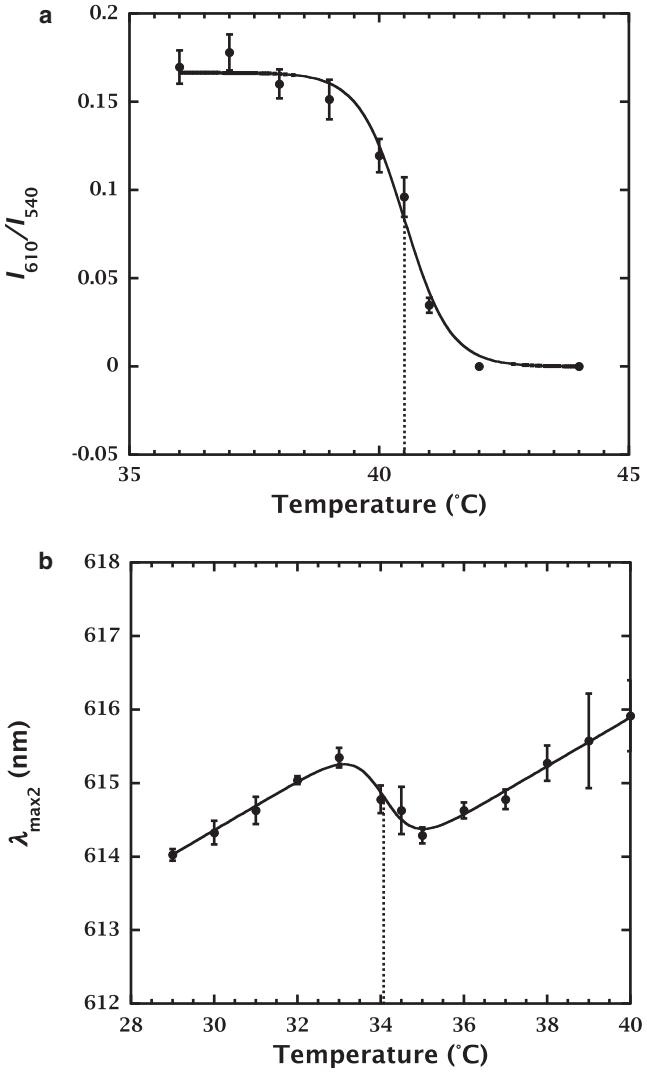

FIGURE 3 Change in phase-sensitive spectral parameters as a function of temperature. Emission spectra of NBD-R595 (0.92 μM) mixed with DPPC LUVs (326 μM) were collected at different temperatures for these plots. (*a*) Change in I_{610}/I_{540} as a function of temperature. The T_m of DPPC determined by sigmoidal fitting (*solid line*) was 40.5 $\pm$ 0.1°C. (*b*) Change in λ_{max2} as a function of temperature. The T_{pre} of DPPC determined by sigmoidal fitting (*solid line*) was 34.1 $\pm$ 0.1°C.

considered two other possibilities for the origin of the 610 nm peak of NBD-R595 in gel-phase LUV. The simplest was a red-edge excitation shift due to the high viscosity of the gel-phase (54). This explanation seems unlikely, because, even in glycerol, which is ~900-fold more viscous than water, no red-shifted peak appeared in the emission spectrum (data not shown). The other possibility was that membrane association of the NBD moieties produced a new fluorescent species due, for example, to dipolar interactions arising from electronic excitation. Either simple dimeric association (excimers) or multimeric association (J-aggregates) can cause a bathochromic shift in fluorescence emission spectra.

Dynamic excimers can arise from the association of a ground-state monomer with an excited-state monomer (54). The standard example is pyrene, which exhibits a structured emission in the 380–400 nm wavelength range at low concentrations (monomer emission) and a broad red-shifted emission at 480–500 nm at high concentrations (excimer emission) (55). Diagnostically, for simple excimer formation, the excitation spectra monitored at monomer and excimer emission wavelengths are almost identical (56). This is not the case for NBD-R595, because there are two peaks in the excitation spectrum for emission at 630 nm (Fig. 4 *a*). Because the wavelength of the broad peak centered at 570 nm is longer than 540 nm, it cannot be an excitation peak for the 540 nm emission peak (see Fig. S5).

Static excimers, using the nomenclature of Winnik (55), arise from the association of two fluorophores that are already associated in the ground state before excitation. This association can cause perturbation of both absorption and excitation spectra (55). For simple ground-state dimer formation, one would expect the relative amplitudes of the two excitation peaks to depend on the concentration of the membrane-bound probe and to have an isofluorescence point. Fig. 4 *a* shows no isofluorescence point; the intensity ratio of 570 nm peak to the 470 nm peak did not change significantly even at a very low concentration of NBD-R595 ($\approx$0.0023% compared to concentration of DPPC). This rules out static excimers.

The remaining possibility is J-aggregates (24,25), which are typically composed of several thousand molecules and coherence domains of <20 molecules (30,31), formed because of intermolecular dipolar couplings among excited-state fluorophores (26). J-aggregates are characterized by a J-band that shows a red-shift compared to the relevant monomer band (24,25), and an extremely small Stokes shift (several nm) (32,34,38). The UV/Vis absorption spectrum of NBD-R595 in the presence of gel-phase DPPC LUVs (Fig. 4 *b*) reveals a red-shifted absorption peak at ~570 nm. But, in contrast to archetypal J-aggregates, the peak was broad and weak and the Stokes shift was quite large ($\approx$40 nm). This suggests that the J-aggregates formed from the NBD moieties of NBD-R595 must be of limited size and coherence length (see Discussion).

A major driving force for J-aggregation is π-π interactions between fluorophores (38). This suggested interactions between the π-planes of NBD as the likely cause of J-aggregate formation. Sonoda et al. (57) recently reported that (*E*,*E*,*E*)-1,6-diphenyl-1,3,5-hexatriene derivatives in the solid state can show large red-shifts of 40–50 nm due to strong π-π interactions between the molecules. We thus hypothesized that the positions of the NBD moieties on R595 allows J-aggregates of NBD to form through π-π interactions. Although J-aggregates have never been reported for NBD as far as we are aware, we considered the possibility that J-aggregates could form simply by restraining NBD at the bilayer interface. We tested this possibility by collecting fluorescence spectra of NBD-lysoPPE, which has a single NBD attached to the ethanolamine headgroup. Only a single

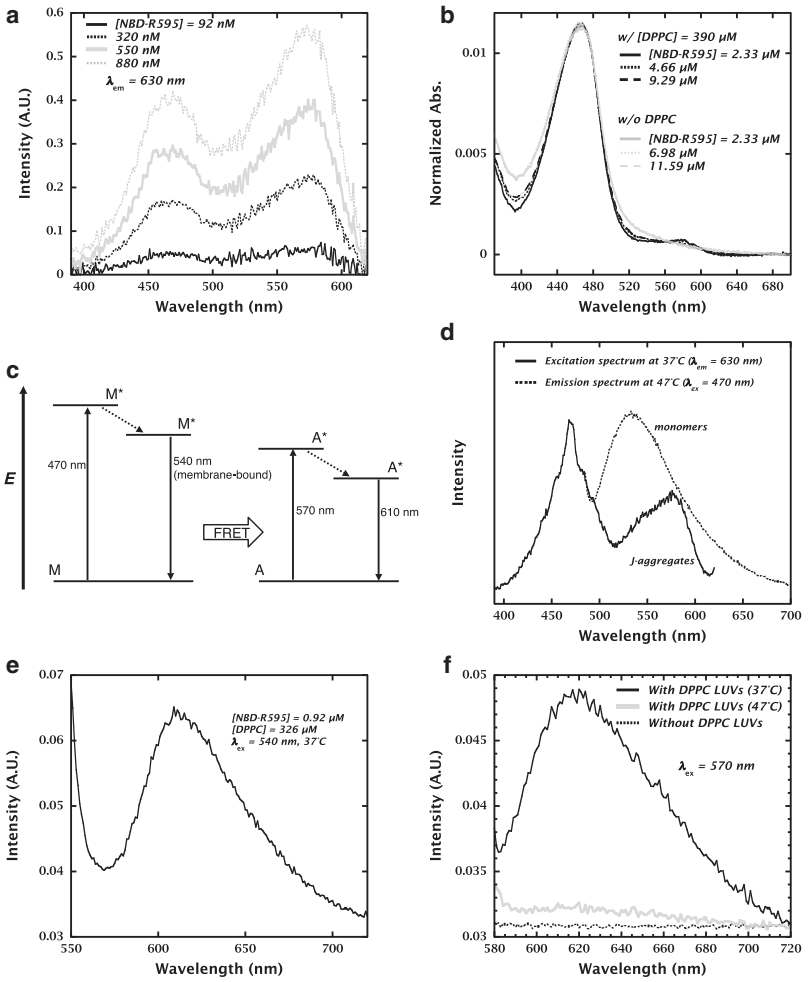

FIGURE 4 Fluorescence and UV/Vis absorbance of NBD-R595 under various conditions. (*a*) Excitation spectra of NBD-R595 at different concentrations in the presence of DPPC LUVs (4 mM) at 37°C. Solid-black, dotted-black, solid-gray, and dotted-gray lines represent the spectra collected for NBD-R595 at 92 nM, 320 nM, 550 nM, and 880 nM, respectively. Intensities have been corrected to account for the wavelength dependence of the intensity of excitation light, by using the data collected with Rhodamine B and Nile Blue (64). The spectra were collected for 630 nm emission to minimize the contribution of 540 nm emission peak. (*b*) UV/Vis absorption spectra of NBD-R595 at different concentrations in the presence (*black lines*) and absence (*gray lines*) of DPPC LUVs (390 μM) at room temperature. Solid-black, dotted-black, and broken-black lines represent the NBD-R595 spectra at 2.33 μM, 4.66 μM, and 9.29 μM, respectively. Solid-gray, dotted-gray, and broken-gray lines represent the spectra at 2.33 μM, 6.98 μM, and 11.59 μM, respectively. Absorbance has been normalized to account for differences in concentration of the fluorescent probe. (*c*) Schematic Jablonski diagram for NBD moiety in DPPC-partitioned NBD-R595. *M* and *M** are monomeric NBDs in ground-state and in excited-state, respectively. Ground- and excited-state NBDs, aggregated with the neighboring NBDs, are depicted as *A* and *A**, respectively. (*d*) Spectral overlap between the excitation spectrum of NBD J-aggregates and the emission spectrum of NBD monomers (in the membrane-bound state). Solid line shows excitation spectrum containing J-aggregate peak around 570 nm. Dotted line shows emission spectrum of NBD-R595 in the presence of fluid-phase DPPC LUVs. Most of NBD moieties do not form J-aggregates on the surface of fluid-phase DPPC LUVs (see panel *f*). To make the spectral overlap clear, the excitation spectrum of NBD-R595 has been scaled by the factor of 2. (*e*) Emission spectrum of NBD-R595 (0.92 μM) mixed with DPPC LUVs (326 μM) at 37°C. (*f*) Comparison of the emission spectra of NBD-R595 (0.92 μM) in DPBS (pH 7.2) with and without DPPC LUVs at 37 and 47°C. Spectra collected in the presence and absence of DPPC LUVs (703 μM) at 37°C ($<T_m$) are drawn as solid-black and dotted-black lines, respectively. Emission in the presence of fluid DPPC LUVs (703 μM) at 47°C is drawn as a solid-gray line. Excitation wavelength was 570 nm.

excitation peak at 470 nm was observed when NBD-lysoPPE was partitioned into DPPC below T_m ($T = 37$°C; Fig. 2 *c*). This means that the mere presence of NBD in a gel-phase bilayer interface is not sufficient for J-aggregation, suggesting that R595 plays a key role in organizing the NBD moieties into J-aggregates. Anchoring of the NBD-R595 hydrocarbon chains in membranes (58) seems to keep the orientation of core sugars vertical to the membrane normal, which could allow the NBD moieties to associate loosely in some complex way to form J-aggregates.

The hypothesis that the NBD moieties of NBD-R595 form J-aggregates in the DPPC membrane interface explains the origin of 610 nm peak. But it does not explain why two peaks were observed in the emission spectrum of NBD-R595 below the DPPC phase transition temperature (Fig. 2 *b*). The logical explanation is the presence of FRET between monomeric NBD moieties and NBD J-aggregates (Fig. 4 *c*). This conclusion is supported by the data of Fig. 4 *d*, which show that the monomer emission spectrum overlaps the J-aggregate excitation spectrum. It is further supported by the observation that direct excitation at 540 nm generates an emission peak at 610 nm from NBD-R595 in the presence of DPPC LUVs (Fig. 4 *e*).

The NBD-R595 excitation spectrum (Fig. 4 *a*) implies that excitation at 570 nm should be sufficient to generate the 610 nm emission peak without the intervention of FRET. Fig. 4 *f* confirms this conclusion. No 610 nm peak was seen in the absence of DPPC LUVs, whereas, in the presence of DPPC at $T < T_m$, an intense emission peak appeared at 618 nm. An important new feature of NBD-R595 fluorescence became apparent when T was raised above the DPPC T_m: A weak peak was observed at 615 nm, suggesting that J-aggregation can occur to a small extent even in fluid-state membranes. These data suggest that NBD-R595 J-aggregates are present in any lipid phase-state and that the J-aggregate coherence length is extremely sensitive to the physical state of the lipid (see Discussion). To explore this idea further, the fluorescence of NBD-R595 (570 nm excitation) was examined in two- and three-component LUVs known to form different phase states.

Changes in the physical state of two- or three-component lipid LUVs detected by NBD-R595

To assess the usefulness of NBD-R595 as an indicator of the physical state of two- or three-component lipid LUVs, we partitioned NBD-R595 into LUVs made from various lipid mixtures comprised of DSPC, DOPC, and cholesterol. We chose this mixture because Feigenson's group (12) has shown that the phases of DSPC-DOPC-cholesterol GUVs change in an intricate way that depends on the mole ratio of the components at 23°C (Fig. 5 *a*). However, we did not expect the phase changes of LUVs to be exactly the same as those of GUVs, for two reasons. First, phase changes of GUVs (12) were determined by fluorescence microscopy using fluorophores that are quite different from NBD-R595. Second, there is no a priori reason that the phase behavior of the macroscopic GUV system should be exactly the same as that of the microscopic LUV system. It is possible, for example, that vesicle radius of curvature is important. Nevertheless, we used the GUV phase diagram of Feigenson's group as a general guide without expecting that the LUV phase behavior would agree in minute detail with GUV phase behavior.

We first examined the base of the triangular phase diagram (Fig. 5 *a*) using DSPC-DOPC mixtures alone (i.e., no cholesterol; Fig. 5 *b*). A plot of the emission intensity at 620 nm (I_{620}; Fig. 5 *c*) revealed a change in slope at ~60 mol % DSPC, suggesting a phase boundary of some kind. In a second experimental series, we examined NBD-R595 fluorescence at various DSPC/DOPC ratios at a fixed cholesterol content of 20 mol % (Fig. 5, *d* and *e*). In this case, the I_{620} increases smoothly but nonlinearly as DSPC content increased from 0 to 75 mol % (Fig. 5 *e*). Finally, we examined I_{620} for a fixed DSPC/DOPC ratio (65/35) as the mol % of cholesterol was varied from 0 to 45 mol % (Fig. 5, *f* and *g*). Because significant changes in I_{620} occurred as a result of relatively small changes in cholesterol concentration, we found it necessary to increase the density of measurements along this line up to ~16 mol %. After 16 mol %, the intensities seemed to decrease linearly with increases in cholesterol content. The plot of I_{620} versus mol % cholesterol thus suggests the possibility of two phase-boundaries, one at ~4 mol % and another at 16 mol % cholesterol (Fig. 5 *g*), but we cannot rule out the possibility that additional discontinuities might appear if the cholesterol concentration is incremented in smaller steps beyond 16 mol %. In any case, the data of Fig. 5 reveal that NBD-R595 fluorescence is quite sensitive to the composition of DSPC-DOPC-cholesterol LUVs.

DISCUSSION

We have described the synthesis and properties of a novel membrane-active fluorescent probe, NBD-R595 (Fig. 1), which is sensitive to the physical state of LUV bilayers. The probe was easily prepared by linking an NBD fluorophore to each of the two amine groups of R595. NBD-R595 partitions strongly and about equally well into LUVs above and below T_m of the lipid host. Because of the high quantum yield of NBD and its high partition coefficient, the membrane-bound probe yielded strong fluorescence signals with virtually no interference from the aqueous-phase monomers. In buffer alone, NBD-R595 had an excitation maximum at 470 nm and a simple log-normal emission curve with a λ_{max} of 565 nm (see Fig. S1). Partitioning of NBD-R595 into fluid-phase or gel-phase lipid vesicles caused an increase in quantum yield and a blue-shift of λ_{max} from 565 nm to 540 nm (Fig. 2).

Remarkably, below the T_m of DPPC, an additional emission peak appeared at ~610 nm (Fig. 2 *b*). This red-shifted peak can also be described by a simple log-normal distribution, which allows the emission spectra below T_m to be decomposed (see Fig. S4) into two emission curves with λ_{max} values of ~540 (λ_{max1}) and 610 (λ_{max2}) nm and temperature-dependent intensities of I_{610} and I_{540} (see Fig. S3). Plots of λ_{max2} and I_{610}/I_{540} versus temperature yielded approximate values for the T_{pre} and T_m of DPPC, respectively (Fig. 3). The estimated transition temperatures were $T_{pre} = 34.1 \pm 0.1$ and $T_m = 40.5 \pm 0.1$°C. In contrast, the corresponding values determined by calorimetric studies are 33.8 and 41.4 ± 0.1°C (59). The two T_{pre} values seem in reasonable agreement, whereas T_m is depressed by 0.9°C. Treating NBD-R595 as a simple impurity and taking into account its membrane concentration, the **e**xpected depression of T_m is ~0.1°C (see Supporting Material). The significantly larger depression that we observed suggests nonideal mixing of NBD-R595 with the host lipid. The broader transitions reported by NBD-R595 compared to that with calorimetric measurements were also consistent with nonideal mixing. The nonideality is not surprising given the complex structure of NBD-R595 (Fig. 1). Regardless of the explanation, these results gave us the first hint of the high sensitivity of NBD-R595 to the overall physical state of the host lipid. We suggest that the sensitivity arises in part from the ability of the probe to partition about equally well into fluid-phase and gel-phase lipids.

The fact that NBD was the only fluorophore present in NBD-R595 and that the excitation spectra monitored at the red-shifted emission peak showed two peaks (Fig. 4 *a*) suggested the presence of NBD molecules in two different states on the surface of membranes. One of the states must be due to NBD molecules acting as simple monomers because of the similarity of the NBD-R595 fluorescence spectra in fluid-state DPPC (Fig. 2 *b*) to those of NBD-lysoPPE under all conditions (Fig. 2, *a* and *b*). Because π-π interactions are known to cause red-shifts in fluorescence spectra (57), the second state likely arises from associations of the NBD moieties of NBD-R595. The relative amplitudes of the two peaks in excitation spectra of NBD-R595 (Fig. 4 *a*) are largely independent of the membrane concentration of NBD-R595 and show no isofluorescence point, which rules

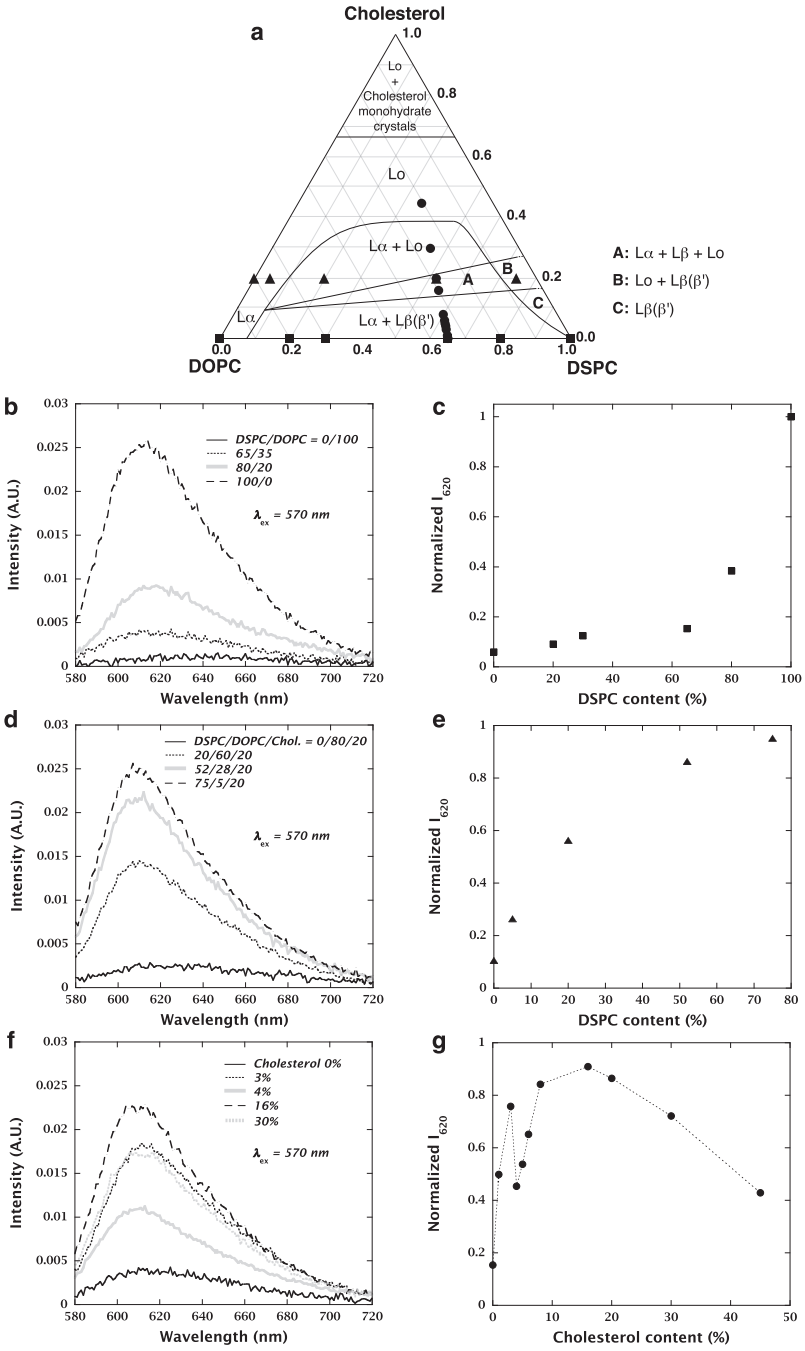

FIGURE 5 Spectral changes in fluorescence emission of NBD-R595 in various DSPC-DOPC-cholesterol mixtures. Excitation wavelength for all spectra was 570 nm. (*a*) The phase diagram of DSPC-DOPC-cholesterol mixtures, redrawn from the report of Zhao et al. (12). The mixtures used for the data in panels *b*–*g* are depicted in this diagram. (*b*) Emission spectra of NBD-R595 (0.94 μM) in the presence of DSPC-DOPC LUVs (197 μM) composed of different DSPC/DOPC molecular ratios (*solid squares*) at 23°C. Solid-black, dotted-black, solid-gray, and broken-black lines represent the spectra in the presence of LUVs whose DSPC contents are 0 mol %, 65 mol %, 80 mol %, and 100 mol %, respectively. (*c*) Change in I_{620} as a function of DSPC content in DSPC-DOPC LUVs. I_{620} was normalized using the I_{620} in the presence of 100 mol % DSPC LUVs. This normalization procedure was also applied to the data in panels *e* and *g*. (*d*) Emission spectra of NBD-R595 (0.94 μM) in the presence of DSPC-DOPC-cholesterol LUVs (197 μM) composed of different DSPC/DOPC/cholesterol molecular ratios (*solid triangles*) at 23°C. Cholesterol content was kept at 20 mol % in LUVs. Solid-black, dotted-black, solid-gray, and broken-black lines represent the spectra in the presence of LUVs whose DSPC/DOPC/cholesterol ratios are 0:80:20, 20:60:20, 52:28:20, and 75:5:20, respectively. (*e*) Change in normalized I_{620} as a function of DSPC content in LUVs containing 20 mol % cholesterol. (*f*) Emission spectra of NBD-R595 (0.94 μM) in the presence of DSPC-DOPC-cholesterol LUVs (197 μM) composed of different DSPC/DOPC/cholesterol molecular ratios (*solid circles*) at 23°C. Cholesterol content was changed keeping DSPC/DOPC ratio to be 65:35 in LUVs. Solid-black, dotted-black, solid-gray, broken-black, and dotted-gray lines represent the spectra in the presence of LUVs whose DSPC/DOPC/cholesterol ratios are 65:35:0, 63:34:3, 62:34:4, 55:29:16, and 45:25:30, respectively. (*g*) Change in normalized I_{620} as a function of cholesterol content in DSPC-DOPC-cholesterol LUVs. The dotted lines between data points were added manually as a visual aid.

out simple dimerization of the NBD groups as the source of the red-shifted peak. Because of the appearance of a red-shifted absorption peak in UV/Vis spectra (Fig. 4 *b*), the most likely source of the red-shifted 610 nm peak is the formation of J-aggregates on the surface of the bilayers formed from the NBD moieties of NBD-R595.

However, the absorption spectra (Fig. 4 *b*) are not consistent with those of typical J-aggregates. The red-shifted absorption at around 570 nm (J-band) is weak and broad, and the Stokes shift is quite large ($\approx$40 nm). We suggest that the J-band inconsistency of NBD-R595 is because of its bulky structure. Typical J-aggregate-forming compounds like cyanine- (24,25) or perylene-based (38) dyes contain few, if any, additional nonfluorescent moieties in the molecules. This makes it possible to form J-aggregates of several thousand molecules with long coherence domains (30,31), causing the appearance of intense J-bands and extremely small Stokes shifts. In contrast, NBD-R595 has hydrocarbon and sugar chains, which are likely to sterically hinder the formation of large J-aggregates of NBD moieties. Because smaller J-aggregates generate broader J-bands and larger Stokes shifts (31,33,34), we surmise that J-aggregates of

NBD-R595 on the surface of DPPC membranes have limited size and coherence length. There are two types of coupling of transition dipole moments that can explain J-aggregate fluorescence: head-to-tail in-line association or coplanar inclined associations (26). We could not distinguish which of these might apply to NBD-R595. Perhaps both are present as a result of the flexibility and only partial ordering of the R595 headgroups. In any case, the R595 headgroups must play a critical role in J-aggregation, because we found no evidence of J-aggregation for NBD-lysoPPE (Fig. 2 *c* and Fig. S6).

We conclude that the red-shifted emission peak that appears in DPPC LUVs for $T < T_m$ (Fig. 2 *b*) is because of FRET between monomeric NBD moieties and NBD-moiety J-aggregates, as summarized in Fig. 4 *c*. As verified by the double peaks in the NBD-R595 excitation spectra (Fig. 4 *a*), the monomers and J-aggregates can be independently excited. This means that the state of the J-aggregates can be monitored by simply exciting membrane-bound NBD-R595 at 570 nm. Indeed, the emission spectrum of the probe excited at this wavelength is quite sensitive to the physical state of DPPC (Fig. 4 *f*). What is the cause of this sensitivity? Although optical spectra of J-aggregates of cyanine dyes in micelles and bilayers depend to some extent on the host surfactant (31,34), the spectra inevitably showed the characteristic narrow and intense red-shifted absorption band and extremely small Stokes shift. These strong J-bands imply that dye-dye interactions are stronger than dye-host interactions. We propose that the bulky R595 headgroup has a strong disruptive influence on J-aggregate formation, but, because J-aggregation can have such profound effects on optical spectra, even small degrees of J-aggregation must have readily observed spectral consequences. We believe that the extreme sensitivity of NBD-R595 to lipid state arises because the J-aggregates are on the margin of stability, causing small changes in local environment to have easily observed spectroscopic consequences.

The sensitivity of NBD-R595 to lipid physical-state was revealed by an exploration of a phase diagram for DSPC-DOPC-cholesterol lipid mixtures determined for GUVs using multiple fluorescent dyes and microscopic measurements (7–14). The objective of these measurements was not to construct a complete phase diagram or to validate the phase diagram determined using GUV. Rather, we sought simply to establish the sensitivity of NBD-R595 to the composition of a three-component lipid mixture. For this purpose, we prepared DSPC-DOPC-cholesterol mixtures dispersed as LUVs in buffer containing NBD-R595 to sample the GUV-determined phase diagram using fluorescence stimulated by 570 nm excitation (Fig. 5 *a*). In the absence of cholesterol, the intensity of fluorescence at 620 nm (I_{620}) increased gradually with DSPC concentration until ~60 mol %, then increased strongly, but linearly, for concentrations >60 mol % (Fig. 5, *b* and *c*). This suggests a phase boundary at ~60 mol %, which was not seen in the GUV phase diagram. But it is consistent with a previous report based on calorimetric studies (60). At room temperature, DSPC and DOPC form monotectic mixtures, in which fluid DOPC mixes with nonfluid DSPC to some extent, but not the reverse. Our results suggest that, as the DSPC concentration increases, I_{620} increases slowly until the DSPC-rich phase becomes the dominant phase at ~60 mol %. We speculate that, in this phase, the J-aggregation becomes more favorable, causing I_{620} to increase more steeply with DSPC concentration.

In the presence of 20 mol % cholesterol, the DSPC-content dependence of I_{620} changed drastically (Fig. 5, *d* and *e*). This may be because of the tendency of cholesterol to have a lipid-condensing effect on DOPC and a fluidizing effect on DSPC (61). When the DSPC/DOPC molar ratio was fixed at 65/35 and the cholesterol content was increased, the behavior of I_{620} became even more complicated (Fig. 5, *f* and *g*). I_{620} tended, at low concentrations, to increase linearly with cholesterol until ~4 mol %, drop abruptly, increase again until ~16 mol %, and then decline linearly. Based on x-ray studies of 1:1 DSPC/DOPC (12) and the phase diagram of DPPC-cholesterol mixtures derived from calorimetry (62), we speculate that the break at 4 mol % cholesterol corresponds to an $L_{\beta'}$–L_{β} transition of a DSPC-rich phase that was enhanced by a condensing effect of cholesterol up to 16 mol %. The cause of the break at 16 mol % is uncertain, but it may be because of the fluidizing effect of cholesterol on DSPC described by Scherfeld et al. (61). Fig. 4 *f* shows, for example, that I_{620} decreases dramatically when DPPC enters the fluid state. If cholesterol begins to fluidize DSPC at 16 mol % cholesterol, then, we speculate, I_{620} would decrease as a result.

Although we can only speculate about the causes of the changes in the NBD-R595 fluorescence at 620 nm, our limited exploration of the DSPC-DOPC-cholesterol phase diagram obtained using GUV behavior as a guide reveals that NBD-R595 is very sensitive to the phase behaviors of one-, two-, and three-component lipid LUVs. NBD-R595 may therefore prove useful for developing LUV phase diagrams when used in combination with complementary data from calorimetric and x-ray measurements.

SUPPORTING MATERIAL

Six figures are available at http://www.biophysj.org/biophysj/supplemental/S0006-3495(09)00681-X.

We thank Dr. Sergei Balashov (University of California at Irvine) for the advice in fluorescence measurements, Michael Myers for his editorial assistance, and the Theory and Experiments in Membrane Protein Organization group for useful discussions.

This work was supported by the LIPID MAPS Large-Scale Collaborative Grant GM-069338 and by GM-74637 from the National Institute of Health.

REFERENCES

1. Singer, S. J., and G. L. Nicolson. 1972. The fluid mosaic model of the structure of cell membranes. *Science*. 175:720–731.

2. Dupuy, A. D., and D. M. Engelman. 2008. Protein area occupancy at the center of the red blood cell membrane. *Proc. Natl. Acad. Sci. USA.* 105:2848–2852.
3. Feigenson, G. W. 2007. Phase boundaries and biological membranes. *Annu. Rev. Biophys. Biomol. Struct.* 36:63–77.
4. Kusumi, A., C. Nakada, K. Ritchie, K. Murase, K. Suzuki, et al. 2005. Paradigm shift of the plasma membrane concept from the two-dimensional continuum fluid to the partitioned fluid: high-speed single-molecule tracking of membrane molecules. *Annu. Rev. Biophys. Biomol. Struct.* 34:351–378.
5. Engelman, D. M. 2005. Membranes are more mosaic than fluid. *Nature.* 438:578–580.
6. Simons, K., and E. Ikonen. 1997. Functional rafts in cell membranes. *Nature.* 387:569–572.
7. Veatch, S. L., and S. L. Keller. 2002. Organization in lipid membranes containing cholesterol. *Phys. Rev. Lett.* 89:268101.
8. Veatch, S. L., and S. L. Keller. 2003. Separation of liquid phases in giant vesicles of ternary mixtures of phospholipids and cholesterol. *Biophys. J.* 85:3074–3083.
9. Veatch, S. L., I. V. Polozov, K. Gawrisch, and S. L. Keller. 2004. Liquid domains in vesicles investigated by NMR and fluorescence microscopy. *Biophys. J.* 86:2910–2922.
10. Veatch, S. L., and S. L. Keller. 2005. Miscibility phase diagrams of giant vesicles containing sphingomyelin. *Phys. Rev. Lett.* 94:148101.
11. Veatch, S. L., K. Gawrisch, and S. L. Keller. 2006. Closed-loop miscibility gap and quantitative tie-lines in ternary membranes containing diphytanoyl PC. *Biophys. J.* 90:4428–4436.
12. Zhao, J., J. Wu, F. A. Heberle, T. T. Mills, P. Klawitter, et al. 2007. Phase studies of model biomembranes: complex behavior of DSPC/DOPC/cholesterol. *Biochim. Biophys. Acta.* 1768:2764–2776.
13. Veatch, S. L., O. Soubias, S. L. Keller, and K. Gawrisch. 2007. Critical fluctuations in domain-forming lipid mixtures. *Proc. Natl. Acad. Sci. USA.* 104:17650–17655.
14. Feigenson, G. W., and J. T. Buboltz. 2001. Ternary phase diagram of dipalmitoyl-PC/dilauroyl-PC/cholesterol: nanoscopic domain formation driven by cholesterol. *Biophys. J.* 80:2775–2788.
15. Small, D. M. 1986. The Physical Chemistry of Lipids. Plenum Press, New York.
16. Raetz, C. R. H., and C. Whitfield. 2002. Lipopolysaccharide endotoxins. *Annu. Rev. Biochem.* 71:635–700.
17. Glauser, M. P., G. Zanetti, J.-D. Baumgartner, and J. Cohen. 1991. Septic shock: Pathogenesis. *Lancet.* 338:732–736.
18. Parrillo, J. E., M. M. Parker, C. Natanson, A. F. Suffredini, R. L. Danner, et al. 1990. Septic shock in humans: advances in the understanding of pathogenesis, cardiovascular dysfunction, and therapy. *Ann. Intern. Med.* 113:227–242.
19. Mueller, M., B. Lindner, S. Kusumoto, K. Fukase, A. B. Schromm, et al. 2004. Aggregates are the biologically active units of endotoxin. *J. Biol. Chem.* 279:26307–26313.
20. Takayama, K., D. H. Mitchell, Z. Z. Din, P. Mukerjee, C. Li, et al. 1994. Monomeric Re lipopolysaccharide from *Escherichia coli* is more active than the aggregated form in the *Limulus* amebocyte lysate assay and in inducing Egr-1 mRNA in murine peritoneal macrophages. *J. Biol. Chem.* 269:2241–2244.
21. Takayama, K., Z. Z. Din, P. Mukerjee, P. H. Cooke, and T. N. Kirkland. 1990. Physicochemical properties of the lipopolysaccharide unit that activates B lymphocytes. *J. Biol. Chem.* 265:14023–14029.
22. Sasaki, H., and S. H. White. 2008. Aggregation behavior of an ultrapure lipopolysaccharide that stimulates TLR-4 receptors. *Biophys. J.* 95:986–993.
23. Ladokhin, A. S., S. Jayasinghe, and S. H. White. 2000. How to measure and analyze tryptophan fluorescence in membranes properly, and why bother? *Anal. Biochem.* 285:235–245.
24. Scheibe, G. 1936. Variability of the absorption spectra of some sensitizing dyes and its cause. *Angew. Chem.* 49:563.
25. Jelley, E. E. 1936. Spectral absorption and fluorescence of dyes in the molecular state. *Nature.* 138:1009–1010.
26. Kasha, M., H. R. Rawls, and M. A. El-Bayoumi. 1965. The exciton model in molecular spectroscopy. *Pure Appl. Chem.* 11:371–392.
27. Sundström, V., T. Gillbro, R. A. Gadonas, and A. Piskarskas. 1988. Annihilation of singlet excitons in J aggregates of pseudoisocyanine (PIC) studied by pico- and subpicosecond spectroscopy. *J. Chem. Phys.* 89:2754–2762.
28. Yao, H., S. Sugiyama, R. Kawabata, H. Ikeda, O. Matsuoka, et al. 1999. Spectroscopic and AFM studies on the structures of pseudoisocyanine *J* aggregates at a mica/water interface. *J. Phys. Chem. B.* 103:4452–4456.
29. Sato, T., M. Kurahashi, and Y. Yonezawa. 1993. Luminescence properties of liposomes incorporating two kinds of cyanine dyes: excitation energy transfer between J-aggregates. *Langmuir.* 9:3395–3401.
30. van Burgel, M., D. A. Wiersma, and K. Duppen. 1995. The dynamics of one-dimensional excitons in liquids. *J. Chem. Phys.* 102:20–33.
31. De Rossi, U., S. Daehne, and M. Lindrum. 1996. Increased coupling size in J-aggregates through *N-n*-alkyl betaine surfactants. *Langmuir.* 12:1159–1165.
32. Yao, H., M. Omizo, and N. Kitamura. 2000. Mesoscopic string structures of thiacyanine J aggregates in solution. *Chem. Commun. (Camb.).* 2000:739–740.
33. Muenter, A. A., D. V. Brumbaugh, J. Apolito, L. A. Horn, F. C. Spano, et al. 1992. Size dependence of excited-state dynamics for J-aggregates at AgBr interfaces. *J. Phys. Chem.* 96:2783–2790.
34. Sidorowicz, A., C. Mora, S. Jablonka, A. Pola, T. Modrzycka, et al. 2005. Spectral properties of two betaine-type cyanine dyes in surfactant micelles and in the presence of phospholipids. *J. Mol. Struct.* 744–747:711–716.
35. Hemenger, R. P. 1977. A theory of optical absorption by aggregates of large molecules. *J. Chem. Phys.* 66:1795–1801.
36. Knapp, E. W. 1984. Lineshapes of molecular aggregates. Exchange narrowing and intersite correlation. *Chem. Phys.* 85:73–82.
37. Scherer, P. O. J., and S. F. Fischer. 1984. On the theory of vibronic structure of linear aggregates. Application to pseudoisocyanine (PIC). *Chem. Phys.* 86:269–283.
38. Kaiser, T. E., H. Wang, V. Stepanenko, and F. Würthner. 2007. Supramolecular construction of fluorescent J-aggregates based on hydrogen-bonded perylene dyes. *Angew. Chem. Int. Ed.* 46:5541–5544.
39. Brade H., Opal S. M., Vogel S. N., and Morrison D. C., editors. 1999. Endotoxin in Health and Disease. Marcel Dekker, New York.
40. Wilkinson, S. G. 1996. Bacterial lipopolysaccharides—themes and variations. *Prog. Lipid Res.* 35:283–343.
41. Wiström, C. A., G. M. Jones, P. S. Tobias, and L. A. Sklar. 1996. Fluorescence resonance energy transfer analysis of lipopolysaccharide in detergent micelles. *Biophys. J.* 70:988–997.
42. Komuro, T., and R. Nakazawa. 1993. Detection of low molecular size lipopolysaccharide contaminated in dialysates used for hemodialysis therapy with polyacrylamide gel electrophoresis in the presence of sodium deoxycholate. *Int. J. Artif. Organs.* 16:245–248.
43. Komuro, T., and C. Galanos. 1988. Analysis of *Salmonella* lipopolysaccharides by sodium deoxycholate-polyacrylamide gel electrophoresis. *J. Chromatogr.* 450:381–387.
44. Stillwell, W., L. J. Jenski, M. Zerouga, and A. C. Dumaual. 2000. Detection of lipid domains in docosahexaenoic acid-rich bilayers by acyl chain-specific FRET probes. *Chem. Phys. Lipids.* 104:113–132.
45. Ladokhin, A. S., J. M. Isas, H. T. Haigler, and S. H. White. 2002. Determining the membrane topology of proteins: insertion pathway of a transmembrane helix of annexin 12. *Biochemistry.* 41:13617–13626.
46. Ghosh, P. B., and M. W. Whitehouse. 1968. 7-Chloro-4-nitrobenzene-2-oxa-1,3-diazole: a new fluorigenic reagent for amino acids and other amines. *Biochem. J.* 108:155–156.
47. Fery-Forgues, S., J.-P. Fayet, and A. Lopez. 1993. Drastic changes in the fluorescence properties of NBD probes with the polarity of the

medium: Involvement of a TICT state? *J. Photochem. Photobiol. A: Chem.* 70:229–243.

48. Mayer, L. D., M. J. Hope, and P. R. Cullis. 1986. Vesicles of variable sizes produced by a rapid extrusion procedure. *Biochim. Biophys. Acta.* 858:161–168.
49. Bartlett, G. R. 1959. Phosphorus assay in column chromatography. *J. Biol. Chem.* 234:466–468.
50. Lewis, R. N. A. H., N. Mak, and R. N. McElhaney. 1987. A differential scanning calorimetric study of the thermotropic phase behavior of model membranes composed of phosphatidylcholines containing linear saturated fatty acyl chains. *Biochemistry.* 26:6118–6126.
51. White, S. H., W. C. Wimley, A. S. Ladokhin, and K. Hristova. 1998. Protein folding in membranes: determining energetics of peptide-bilayer interactions. *Methods Enzymol.* 295:62–87.
52. Vincent, M., B. de Foresta, and J. Gallay. 2005. Nanosecond dynamics of a mimicked membrane-water interface observed by time-resolved Stokes shift of LAURDAN. *Biophys. J.* 88:4337–4350.
53. Koynova, R., and M. Caffrey. 1998. Phases and phase transitions of the phosphatidylcholines. *Biochim. Biophys. Acta.* 1376:91–145.
54. Lakowicz, J. R. 1999. Principles of Fluorescence Spectroscopy. Kluwer Academic/Plenum Publishers, New York.
55. Winnik, F. M. 1993. Photophysics of preassociated pyrenes in aqueous polymer solutions and in other organized media. *Chem. Rev.* 93: 587–614.
56. Zagrobelny, J., T. A. Betts, and F. V. Bright. 1992. Steady-state and time-resolved fluorescence investigations of pyrene excimer formation in supercritical CO_2. *J. Am. Chem. Soc.* 114:5249–5257.
57. Sonoda, Y., M. Goto, S. Tsuzuki, and N. Tamaoki. 2006. Fluorescence spectroscopic properties and crystal structure of a series of donor-acceptor diphenylpolyenes. *J. Phys. Chem. A.* 110:13379–13387.
58. Levine, D. M., T. S. Parker, T. M. Donnelly, A. Walsh, and A. L. Rubin. 1993. *In vivo* protection against endotoxin by plasma high density lipoprotein. *Proc. Natl. Acad. Sci. USA.* 90:12040–12044.
59. Lichtenberg, D., M. Menashe, S. Donaldson, and R. L. Biltonen. 1984. Thermodynamic characterization of the pretransition of unilamellar dipalmitoyl-phosphatidylcholine vesicles. *Lipids.* 19:395–400.
60. Phillips, M. C., B. D. Ladbrooke, and D. Chapman. 1970. Molecular interactions in mixed lecithin systems. *Biochim. Biophys. Acta.* 196: 35–44.
61. Scherfeld, D., N. Kahya, and P. Schwille. 2003. Lipid dynamics and domain formation in model membranes composed of ternary mixtures of unsaturated and saturated phosphatidylcholines and cholesterol. *Biophys. J.* 85:3758–3768.
62. McMullen, T. P. W., and R. N. McElhaney. 1995. New aspects of the interaction of cholesterol with dipalmitoylphosphatidylcholine bilayers as revealed by high-sensitivity differential scanning calorimetry. *Biochim. Biophys. Acta.* 1234:90–98.
63. Leidy, C., W. F. Wolkers, K. Jørgensen, O. G. Mouritsen, and J. H. Crowe. 2001. Lateral organization and domain formation in a two-component lipid membrane system. *Biophys. J.* 80:1819–1828.
64. Balashov, S. P., E. S. Imasheva, J. M. Wang, and J. K. Lanyi. 2008. Excitation energy-transfer and the relative orientation of retinal and carotenoid in Xanthorhodopsin. *Biophys. J.* 95:2402–2414.